Dalton Transactions

Deciphering the structure and the potassium ions transport mechanism of potassium borate glass

Journal:	*Dalton Transactions*
Manuscript ID	DT-ART-03-2024-000804.R1
Article Type:	Paper
Date Submitted by the Author:	24-Apr-2024

Complete List of Authors:	Song, Lulu; Qinghai Institute of Salt Lakes Chinese Academy of Sciences, Qinghai Institute of Salt Lakes Hannon, Alex; Rutherford Appleton Laboratory, ISIS Facility Feller, Steve; Coe College, Physics Liu, Ruirui; Lanzhou University, McGuire, Peyton; Coe College Zhang, Bo; Qinghai Institute of Salt Lakes Chinese Academy of Sciences, Key Laboratory of Comprehensive and Highly Efficient Utilization of Salt Lake Resources Zhou, Yongquan; Qinghai Institute of Salt Lakes Chinese Academy of Sciences Li, Wu; Qinghai Institute of Salt Lakes Chinese Academy of Sciences Zhu, Fayan; Qinghai Institute of Salt Lakes Chinese Academy of Sciences

Deciphering the structure and the potassium ions transport mechanism of potassium borate glass

Lulu Song [a, b], Alex C. Hannon [c], Steve Feller [d], Ruirui Liu [a], Peyton McGuire [d], Bo Zhang [a], Yongquan Zhou [a], Wu Li [a, *], Fayan Zhu [a, *]

[a] Key Laboratory of Green and High-end Utilization of Salt Lake Resources, Qinghai Institute of Salt Lakes, Chinese Academy of Sciences, Xining 810008, China

[b] University of Chinese Academy of Science, Beijing 100049, China

[c] ISIS Facility Rutherford Appleton Laboratory, Chilton, Didcot, Oxon OX11 0QX, UK

[d] Coe College, Physics Department, 1220 First Ave NE, Cedar Rapids, IA 52402, USA

ABSTRACT: Potassium borate glass has great potential as ion transport materials. The ion transport rate is closely related to the microstructure of the glass. However, the disorder and variations in boron and oxygen atom types in the glass structure pose challenges in the complex glass structure analysis. In this work, the structure of potassium borate glass was unveiled through neutron diffraction method and ab initio molecular dynamics (AIMD) simulations. The B-O, K-O, and O-O atomic interactions, bond lengths, coordination numbers, cavities distribution, ring structure distributions and other detailed information in the microstructure of potassium borate glass were obtained. By comparing the structure and properties of potassium borate glass and the crystals of similar components, it is found that the bond lengths of ^{3}B-BO (BO, bridging oxygen), ^{4}B-BO and ^{3}B-NBO (NBO, non-bridging oxygen) are longer than those of corresponding crystals, so the structure of boron-oxygen network is looser and the density is smaller than that of similar crystals. Moreover, we found a rule that in both borate glass and crystal, the increase of NBO shortened the length of B-O bond, and the increase of ^{4}B increased the length of B-O bond. The key structures affecting the transport rate of K^{+} were NBO, chain structure units and cavities. This work will provide reference data for designing and developing electrically conductive amorphous materials with faster potassium ion transport rates.

Keywords: Potassium borate glass, Neutron diffraction, Glass structure, K^{+} transport, non-bridging oxygen

1. Introduction

Potassium borate glass is widely used as glass-forming agents [1-5], which can be utilized to design and prepare new materials with potential applications in optics, electrochemistry, radiation shielding, etc. Alkali metal borate glass exhibit excellent

nonlinear optical properties [6], and the borate groups composed of B-O-B bonds contribute to enhancing the optical characteristics of glasses [7]. Currently, radiation shielding materials are popular for their use in various fields such as electricity production, military surveillance, and research activities [8, 9]. Thermoluminescence (TL) is the most basic characteristic of radiation dose materials. Borate glass has excellent thermoluminescence properties, and has better transparency, mechanical strength, and chemical durability [10, 11]. Therefore, it is a high-performance shielding material that is expected to replace concrete. Potassium-ion batteries (PIBs) have advantages such as abundant reserves, low cost, and similar oxidation-reduction potential to lithium-ion batteries (LIBs), making them preferred alternatives to LIBs [12]. The introduction of potassium ions in borate glass helps to improve the strength and electron emission capacity of the glass [13]. In terms of bioactive amorphous materials, the addition of K_2O enhances ion diffusion rates to promote bone formation [14]. The abnormal properties of potassium borate glass depend on its structure, and the diversity of structural units and the variability of K-O and B-O coordination numbers bring challenges to structural analysis.

A variety of techniques have been used to study the complex borate glass structures. Raman spectroscopy indicates that the main structural units present in potassium borate glass include metaborate units, pyroborate units, orthoborate units, boroxol rings, di-borate groups and tetraborate groups [15-19]. ^{11}B NMR experimental results and physical-chemical models suggest that the peak value of N_4 occurs at x = 0.30 [19, 20]. Wright et al. [19] used neutron diffraction to determine the distance of the first coordination shell of B-O interactions in the $0.28K_2O{\cdot}0.72^{11}B_2O_3$ glass structure is ~1.4 Å, with $r_{B\text{-}O(B\emptyset 3)}$ = 1.38 Å and $r_{B\text{-}O(B\emptyset 4\text{-})}$ = 1.46 Å. Umesaki et al. [20] showed that the B-O, K-O and O-O effects in $0.20K_2O{\cdot}0.80^{11}B_2O_3$ glass are 1.39, 2.83 and 2.40 Å, respectively. At higher $B\emptyset_4^-$/NBO ratios, alkali and alkaline earth metal cations primarily act as "network formers", while at higher NBO contents, they primarily act as “network modifiers” [23-26]. Furthermore, at higher NBO contents, the main oxygen atoms in $B\emptyset_4^-$ units are also NBOs [23]. An increase in $B\emptyset_4^-$ content in the glass helps to enhance the thermal and mechanical stability of the glass, while an increase in NBO

results in a denser glass [27]. Because B-NBO bond is longer than B-BO bond [28]. In zinc borate glass, the density increases and the molar volume decreases with increasing ZnO content [29]. In lithium borate glass, the density initially increases and then decreases, while the molar volume decreases with increasing Li_2O content [30]. The arrangement of network modifier atoms in uniformly nucleated glass structures is close to that in crystals of similar component [31, 32]. The study of metallic glass also shows that the medium program structure exists in both glass and crystal [33], and the medium range structure is closely related to magnetic order [34]. The above literature shows that the short and medium-range ordered structure is the key structure of glass, which is crucial for the regulation of microscopic properties. At present, the ion transport mechanism of potassium borate glass as a solid electrolyte remains to be explored, and there is a lack of relevant studies on the effect of short - and medium-range structural changes on the amorphous properties, especially the internal relationship between NBO, $BØ_4^-$ and density, ion transport and other properties is still unclear.

In this work, the neutron diffraction experiment data is obtained by using neutron diffraction method, and the data is analyzed by EPSR and difference subtraction method, and the structure information of potassium borate glass is obtained. Meanwhile, the molecular dynamics simulation method is used to supplement the verification. The effect of glass structure on ion transport, density and molar volume is discussed based on obtaining the structure information of atomic interaction distance and coordination number, ring and chain structure unit, micro cavity distribution and NBO content change. This study provides a reference for revealing the influence of medium and short-range structure on the amorphous properties.

2. Experimental

2.1. Sample preparation and characterization

Using isotope boric acid of analytical purity (purity: 99.27%, company: Eagle-Picher) and potassium carbonate of analytical purity (purity: 99.0%) as raw materials, they were thoroughly mixed in a platinum crucible and then heated in a muffle furnace

at 1000°C for 15 minutes. The temperature was raised to 1100°C and heating continued for 10 minutes. Colorless, transparent, and uniform potassium borate glass samples with the composition of $x\mathrm{K_2O}\cdot(1\text{-}x)^{11}\mathrm{B_2O_3}$ (x = 0.10, 0.20, 0.30, 0.40) were prepared by the quenching method on a flat plate. As potassium borate glass is highly hygroscopic, the prepared samples were first sealed and then stored in a nitrogen atmosphere glove box.

The composition, mass density (ρ_n), atomic density (ρ_a), and molar volume (V_m) of the potassium borate glass are shown in Table 1. The deviation of sample composition caused by mass loss is within ±0.016. References to relevant calculation formulas [30].

Table 1

The composition, mass density, atomic density and molar volume of potassium borate glass

Sample	Nominal composition		Composition from mass loss		ρ_n (iso)	ρ_n (nat)	ρ_a	V_m
	K_2O (x)	$^{11}B_2O_3$	K_2O	$^{11}B_2O_3$	(g·cm^{-3})	(g·cm^{-3})	(Å^{-3})	mol·cm^{-3}
$0.10K_2O\cdot0.90^{11}B_2O_3$	0.1000	0.9000	0.0925	0.9075	2.0200	2.0102	0.0843	35.7310
$0.20K_2O\cdot0.80^{11}B_2O_3$	0.2000	0.8000	0.1958	0.8042	2.1303	2.1211	0.0868	34.7531
$0.30K_2O\cdot0.70^{11}B_2O_3$	0.3000	0.7000	0.2879	0.7121	2.2644	2.2556	0.0900	33.3799
$0.40K_2O\cdot0.60^{11}B_2O_3$	0.4000	0.6000	0.3840	0.6160	2.2788	2.2707	0.0893	33.7523

2.2. Neutron diffraction

Neutron diffraction experiments on potassium borate glass were conducted on the GEM diffractometer at the ISIS Spallation Neutron Source (Rutherford Appleton Laboratory) [35] in the UK. The experiments were carried out in a vacuum-sealed vanadium can at room temperature (inner diameter 8.3 mm, wall thickness 25 μm), considering that the potassium borate glass sample is prone to moisture absorption and deterioration, so try to reduce the contact between the sample and the air during the experiment. The standard ATLAS program [36] was used to correct the data from detector groups 1, 2, 3, 4, and 5 (covering a 2θ range from 5.32° to 107.07°) for background diffraction and container diffraction, multiple diffraction, self-attenuation and inelastic (Placzek) effects to obtain a distinct scattering function *i(Q)*. The neutron diffraction data of the measured vanadium niobium rod was used for data normalization. The *i(Q)*

data underwent Fourier transformation and Lorch correction [37] to obtain the total correlation function *T(r)*. The relevant calculation equation is as follows [38, 39],

The distinct scattering *i*(*Q*) is given by the following equation

$$i(Q) = \sum_{l,l'} \overline{b}_l \overline{b}_{l'} \sum_{\substack{j=1 \\ j \neq k}}^{N_l} \sum_{k=1}^{N_{l'}} \frac{1}{N} \frac{\sin(QR_{jk})}{QR_{jk}} \quad (1)$$

Structural information may then be obtained by a Fourier transformation of *i*(*Q*), yielding the total correlation function

$$T'(\mathrm{r}) = T^0(r) + \frac{2}{\pi} \int_0^\infty Qi(Q)M(Q)sin(rQ)dQ \quad (2)$$

where *M*(*Q*) is a modification function. The average density contribution to the correlation function is

$$T^0(r) = 4\pi r g^0 \left(\sum_l c_l \overline{b_l} \right) \quad (3)$$

The correlation function is a weighted sum of partial correlation functions, $t_{ll'}(r)$

$$T(r) = \sum_{l,l'}^{l \geq l'} c_l (2 - \delta_{ll'}) \overline{b}_l \overline{b}_{l'} t_{l-l'}(r) \quad (4)$$

where the *l,l'* summations are over all unique pairs of elements in the sample.

2.3. Molecular dynamic simulation

Born-Oppenheimer molecular dynamics simulation of potassium borate glass structure was carried out by CP2K program [40]. The generalized gradient approximation and the PBE function were applied [41]. The initial atomic configuration of vitreous potassium borate was generated using packmol [42]. The cubic simulation box at room temperature contains approximately 400 atoms (depending on the composition of each sample, as shown in Table S1) to match the experimental number density. Further optimization is performed using density functional theory (DFT), and the molecularly optimized consistent polarization double-zeta basis set DZVP [43] and Goedecker−Teter−Hutter (GTH) type pseudopotentials [44] are adopted for each atom involved. The FPMD simulation after DFT optimization starts at 298.15 K. A

Nosé−Hoover heat bath [45, 46] with a length of 3 is used in a typical NVT ensemble. Heating from 298.15K to above the glass transition temperature (~ 925 K) to 1398.15 K with a gradient of 400 K, a time step of 1 fs/step, and heating for 10 ~ 20 ps per step. At 1398.15 K, the system is balanced for 20 ps, and it is cooled to 298.15 K with the same temperature step and similar simulation time. Finally balanced for 20 ps at 298.15 K and then data collection. The connectivity and distribution of the ring structure were analyzed using R.I.N.G.S. [47] Pore distribution analysis was carried out using the pyMolDyn [48] program. The Visual Molecular Dynamics (VMD) [49] program was used to analyze the simulated trajectories and visualize them graphically. The ion transport path of K^+ in glass was studied by applying an electric field of 0.02 a.u. along the Z axis and fixing the boron-oxygen network structure.

2.4. Empirical Potential Structure Refinement

The Empirical Potential Structure Refinement (EPSR) method [50] was used to analyze the neutron diffraction experimental data of potassium borate glass. The model uses reference potentials consisting of standard Lennard-Jones plus Coulomb terms. When building the model, approximately 4500 atoms (K, B, O atoms) are placed in a cubic box with periodic boundary conditions. Table 2 lists the Lennard Jones potential parameters, the atomic charges, box composition and box size are listed in Table S2 and Table S3. Before the empirical potential structure refinement, the model undergoes continuous NVT Monte Carlo equilibrium under the reference potential after running to equilibrium at 10000K, and the initial structural model is obtained through a continuous cooling process at 1400K, 1200K, 1000K, 700K, 300K. Then the relaxation balance is performed by adjusting the appropriate ereq value, and the potassium borate glass structure model and smooth pdf data are obtained.

3. Structure and Discussion

3.1. Neutron diffraction data

The interference function of potassium borate glass is shown in Fig. 1, left. As can be seen from the figure, the oscillation amplitude of the *i(Q)* data at high *Q* is very small

and the data is smooth, indicating that the neutron diffraction data of potassium borate glass obtained in this study is of high quality. There are three peaks, Q_0, Q_1, and Q_2, when $0 < Q < 3.7$ Å^{-1}. Q_0 is related to the K-K interaction. With the increase of K_2O content, the corresponding atomic interaction distance decreases (5.61 Å to 5.07 Å), the atomic interaction range indicated by Q_1 and Q_2 increases, and the short and medium range ordered structure increases. The total correlation function of potassium borate glass is shown in the Fig. 1, right. As can be seen from the figure, there are three main interaction peaks, P_1, P_2, and P_3, within the range of 4 Å. The P_1 peak represents B-O interaction. As the content of K_2O increases, the intensity of the P_1 peak decreases, the half-peak width increases, and the r value increases from 1.38 to 1.41 Å. The P_2 peak includes four types of interactions: B-B, O-O, B-O, and K-O. The P_3 peak contains four types of interactions: B-O, O-O, K-K, and K-B. As the content of K_2O increases, the intensity of both P_2 and P_3 peaks decrease, full-width at the half of the maximum (FWHM) increases, and the corresponding r values increase from 2.39 to 2.42 Å, and 3.63 to 3.68 Å, respectively.

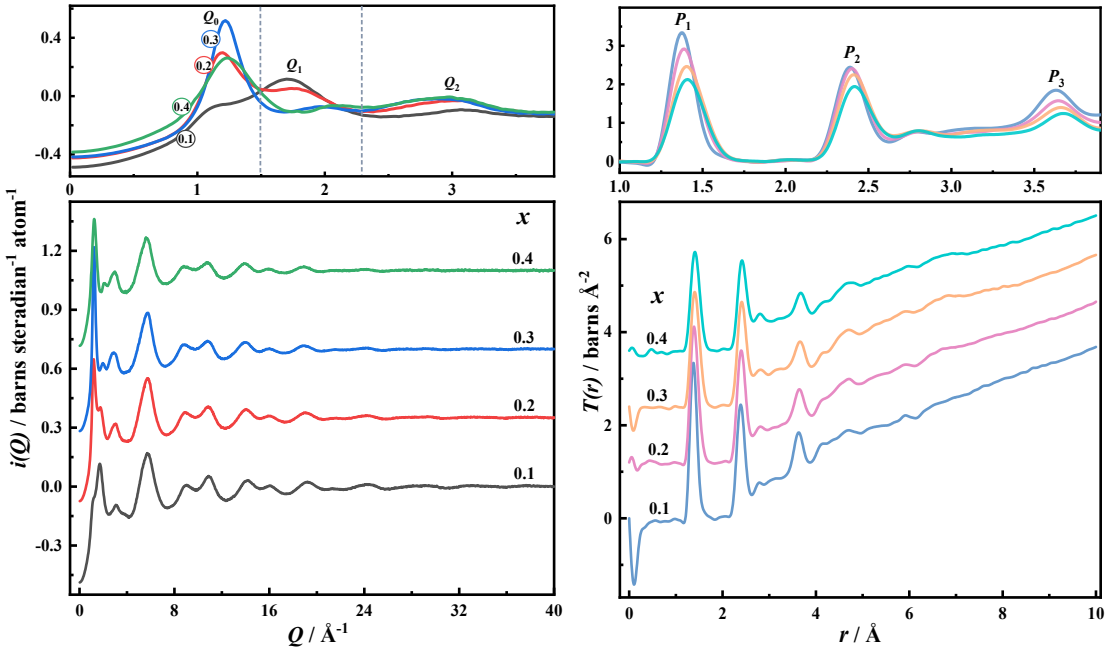

Fig. 1. Left: Interference function $i(Q)$ of potassium borate glass, right: total correlation function $T(r)$ of potassium borate glass

3.2. Analysis of Neutron Experiment Data

3.2.1. The difference method

The potassium borate glass *T(r)* spectrum is very complicated, especially the P_2 and P_3 peaks. Taking $0.1K_2O{\cdot}0.9^{11}B_2O_3$ glass as an example, the first peak in the *T(r)* spectrum has good symmetry and only contains B-O interaction [51]. As shown in the left graph of Fig. 2, the simulations of B-O in the P_2 peak is simulated based on the second coordination shell B-O distance (2.79 Å) in the $g_{B\text{-}O}(r)$ of the AIMD simulation data, and its coordination number and root-mean-square deviation $\langle u_{BO}^2\rangle^{1/2}$ references the neutron and X-ray diffraction data of B_2O_3 glass [52, 53]. The distance and coordination number of the O-O interaction are based on the first coordination shell O-O interaction information in the $g_{O\text{-}O}(r)$ of the AIMD simulation data. By subtracting the simulated $T(r)_{B\text{-}O,\ O\text{-}O}$(simu) from the total $T(r)$exp data, the differential data $T(r)_{B\text{-}B,\ K\text{-}O}$(diff) containing only B-B and K-O interactions, and then the B-B and K-O interactions can be obtained by fitting. The analysis of P_3 peak also adopts the difference method, and the simulation of B-O, O-O and K-B interactions refers to the AIMD simulation results and B_2O_3 glass data [52, 53], which is similar to the analysis process of P_2 peak, as shown in the right graph of Fig. 2. The information of atomic pair interaction distance and coordination number in $xK_2O{\cdot}(1\text{-}x)^{11}B_2O_3$ (x = 0.10, 0.20, 0.30, 0.40) glass is shown in Table S4. As can be seen from the table, with the increase of K_2O content, the B-O distance increases from 1.37 to 1.41 Å, and the O-O action distance changes little. In summary, B-O distance increases with the increase of K_2O content in potassium borate glass, and $r_{B\text{-}O}(B\text{Ø}_4^-)$ = 1.46 Å bond grows larger than $r_{B\text{-}O}(B\text{Ø}_3)$ = 1.38 Å [19], so the increase of B-O distance is closely related to the increase of $B\text{Ø}_4^-$ content. However, the maximum point of the $B\text{Ø}_4^-$ content is x = 0.3 [20], indicating that there are other factors affecting the B-O bond length besides the $B\text{Ø}_4^-$ content, which will be discussed further later.

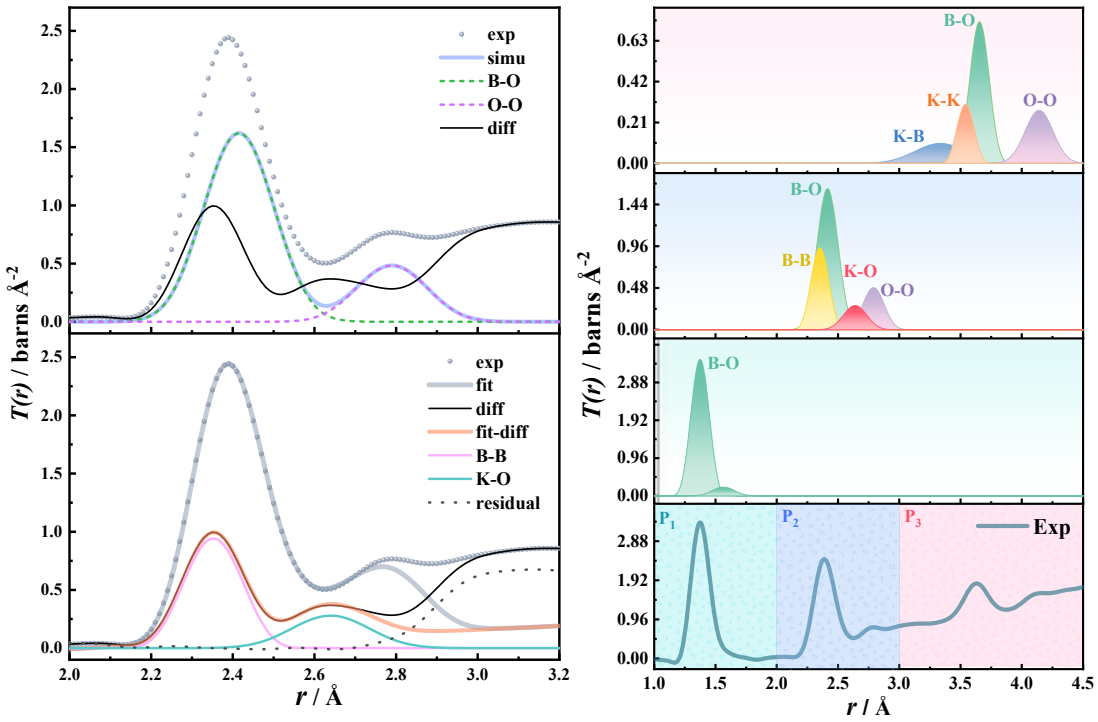

Fig. 2. Real spatial distribution function $T(r)$ of $0.1K_2O{\cdot}0.9^{11}B_2O_3$ glass. Left: the fitting of peak P_2, the top figure is the simulated B-O and O-O peaks, and the lower figure is the B-B and K-O peaks obtained by subtraction; Right: the fitted peaks P_1, P_2 and P_3.

3.2.2. Analysis of PDF data obtained by EPSR and AIMD methods

The $F(Q)$ and $G(r)$ spectra of the experiment and EPSR simulation of potassium borate glass are shown in Fig. S1 (SI). It can be seen from the figure that the EPSR simulation $F(Q)$ and $G(r)$ data overlap well with the neutron experiment data, indicating that the EPSR simulation better presents the experimental data.

B-O interactions

The pair distribution function (PDF) of B-O interactions and B-O bond lengths in different structural units obtained by EPSR and AIMD method is shown in Fig. 3. As shown in the figure, the PDF data obtained by the two methods differ slightly, mainly due to the different calculation principles of the two methods [40, 50] and the box sizes (Tables S1 and S3). The B-O interaction distance of $xK_2O{\cdot}(1\text{-}x)^{11}B_2O_3$ ($0.1 \leq x \leq 0.4$) glass experimental data is 1.37, 1.39, 1.40, 1.41 Å respectively, which are close to the results obtained by AIMD, EPSR and subtraction method (Table S4). In addition, B-O interaction distance increases with the increase of K_2O content. The coordination number distribution of B-O action is shown in Fig. S2. It can be seen from the figure

that with the increase of K_2O content, the B-O coordination number gradually increases, which is consistent with the change trend of B-O coordination number obtained by the difference method (Table S4). The maximum point of the change of the tetra-coordinated boron content (N_4) is located at x = 0.30, accounting for about 30% [20], indicating that the coordination number of B-O interaction is less than 3.5, which is close to the results of B-O coordination number given in this paper. According to the research results given by Koroleva et al. [20], the main basic structural units in potassium borate glass are $B\emptyset_3$ and $B\emptyset_4^-$ when x=0.1 and 0.2. At x=0.3, the $B\emptyset_2O^-$ structural unit begins to appear, and at x=0.4, the $B\emptyset_2O^-$ becomes the main structural unit and the $B\emptyset O_2^-$ structural unit begins to appear. Therefore, the B-O effect in potassium borate glass is mainly tri-coordination, but with the increase of K_2O content, the proportion of NBO in tri-coordination boron is also increasing, and the change of the overall basic structural unit in the glass is that the content of $B\emptyset_3$ decreases, the content of $B\emptyset_4^-$ increases, and the content of $B\emptyset_{(3-a)}O_a^{-a}$ (a=1 or 2) increases. The change in the basic structural unit causes the three-dimensional connectivity of the glass to increase and the boron-oxygen network structure to become dispersed, so the density of the glass increases (Fig. S3).

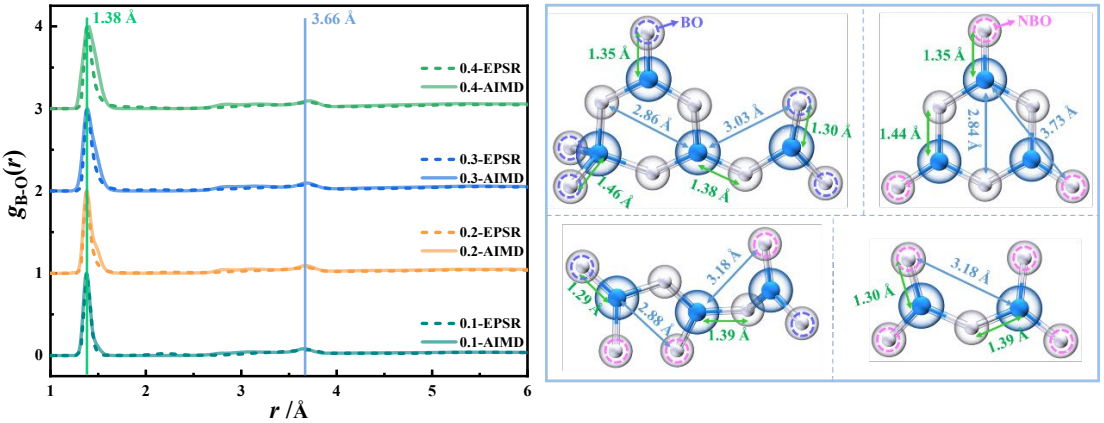

Fig. 3. Pair distribution function of B-O interaction and B-O bond lengths in different structural units in $xK_2O\cdot(1-x)^{11}B_2O_3$ ($0.1 \leq x \leq 0.4$) glass obtained by EPSR and AIMD methods

In this work, the atom labeling method was used to mark ^{3}B, ^{4}B, BO, and NBO atoms in the equilibrium structure simulated by AIMD, respectively. Then four kinds of B-O interactions of ^{3}B-BO, ^{3}B-NBO, ^{4}B-BO, and ^{4}B-NBO were obtained. At the same time, the $K_2B_4O_7$ crystal containing ^{3}B and ^{4}B (the mole content of K_2O is 0.33) and the $K_3B_3O_6$ crystal containing BO and NBO (the mole content of K_2O is 0.50) were

also marked in the same way. As shown in Fig. 4, the related data are shown in Table S5. As can be seen from the figure, there are obvious differences between the structures of the glass and the crystals with similar components: (1) There is a small amount of ^{4}B-NBO interaction in the $0.40K_2O{\cdot}0.60^{11}B_2O_3$ glass, about 2.6%, while there is no such interaction in other glass; (2) The main B-O interaction in the $0.40K_2O{\cdot}0.60^{11}B_2O_3$ glass is ^{3}B-BO, about 57.3%, the ^{4}B-BO interaction is about 23.5% , while the proportions of ^{3}B-BO and ^{4}B-BO interactions in the $K_2B_4O_7$ crystal are very close; (3) The bond lengths of ^{3}B-BO in $0.40K_2O{\cdot}0.60^{11}B_2O_3$ glass, $K_2B_4O_7$, and $K_3B_3O_6$ crystals are 1.40, 1.37, and 1.37Å, respectively. The ^{4}B-BO and ^{3}B-NBO bond lengths (1.49 and 1.35) in the glass are longer than those (1.48, 1.33 Å) in the crystal. In addition, the B-O bond length of the $K_2B_4O_7$ crystal (1.42 Å) is much longer than the B-O bond length of the $K_3B_3O_6$ crystal (1.36 Å). The above information shows that potassium borate glass contains more B-O bond types than similar component crystals, and the bond lengths of ^{3}B-BO, ^{4}B-BO and ^{3}B-NBO are longer than those of corresponding crystals, indicating that the boron-oxygen network of glass is looser than that of similar component crystals. Fig. S3 shows that the density of the glass is smaller than that of the crystals of similar components, confirming the conclusion that the structure of the glass is relatively loose. In both glass and crystal, the increase of NBO decreases the length of B-O bond, and the increase of ^{4}B increases the length of B-O bond. In addition, Eden et al. 's study [23] concluded that the bond lengths of ^{3}B-NBO, ^{3}B-BO, ^{4}B-NBO and ^{4}B-BO in sodium borate glass are 1.34, 1.35, 1.34 and 1.43 Å respectively, and the bond lengths all increase gradually with the increase of Na_2O content. Obviously, the four B-O interactions in the structure of potassium borate glass are longer than the corresponding atomic pairs in sodium borate glass, indicating that the arrangement of B and O atoms in potassium borate glass is looser, which is also the structural reason why the density of potassium borate glass is less than that of sodium borate glass [54].

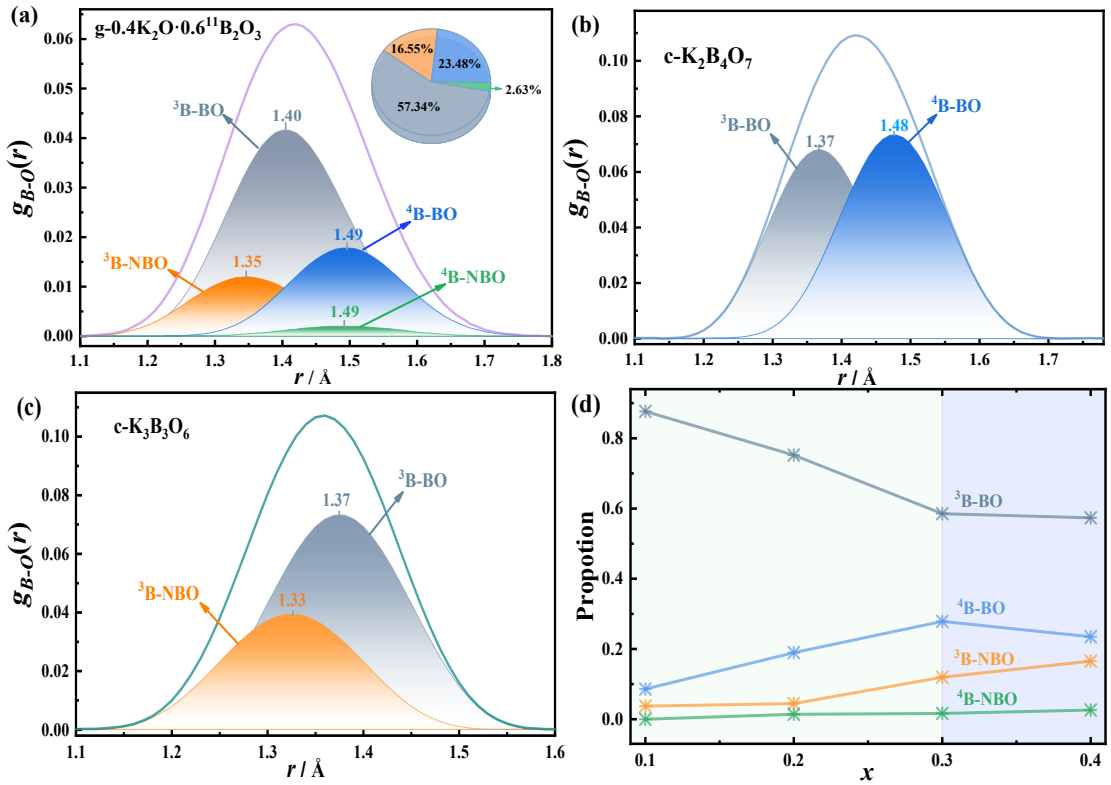

Fig. 4. (a), (b) and (c) represent the distribution of ^{3}B-BO, ^{3}B-NBO, ^{4}B-BO and ^{4}B-NBO interactions in the first coordination layer of the B-O interaction in $0.40K_2O{\cdot}0.60^{11}B_2O_3$ glass and $K_2B_4O_7$, $K_3B_3O_6$ crystal respectively, the fan chart on the right in $0.40K_2O{\cdot}0.60^{11}B_2O_3$ glass shows the percentage of each atom-pair interaction. (d). The relative contents of ^{3}B-BO, ^{3}B-NBO, ^{4}B-BO and ^{4}B-NBO interaction in $xK_2O{\cdot}(1\text{-}x)^{11}B_2O_3$ ($0.1 \leq x \leq 0.4$) glass

The relative contents of the ^{3}B-BO, ^{3}B-NBO, ^{4}B-BO and ^{4}B-NBO interactions in $xK_2O{\cdot}(1\text{-}x)^{11}B_2O_3$ ($0.10 \leq x \leq 0.40$) glass are shown in Fig. 4 (d). $x = 0.30$ is the inflection point of the four interaction changes, which is also the maximum point of the tetra-coordinated boron (^{4}B) content [15, 17, 19]. As can be seen from the figure, ^{3}B-BO has the highest relative content, followed by ^{4}B-BO and ^{3}B-NBO. When $0.10 \leq x \leq 0.30$, with the increase of K_2O content, the ^{3}B-BO interaction significantly decreases, and the ^{3}B-NBO and ^{4}B-BO interactions increase, the total B-O bond length increases. When $0.30 \leq x \leq 0.40$, the ^{3}B-BO interaction changes little, the ^{4}B-BO interaction decreases, the ^{3}B-NBO interaction increases, the ^{4}B content decreases slightly, but a new ^{4}B-NBO interaction is generated, so the total B-O bond length still increases. The maximum point for the content of $B\emptyset_4^-$ ($x = 0.3$) is also the maximum point of density, atomic density, and minimum point of molar volume of potassium borate glass (Fig. S3). On the one hand, due to the increase of $B\emptyset_4^-$ content, the boron-oxygen network connectivity is enhanced, the atomic arrangement of the glass becomes denser, and the

corresponding molar volume decreases. On the other hand, the increase of NBO content (Fig. S4) and the length of B-NBO bond are shorter than B-BO bond led to the shortening of the distance between B and O atoms in the boron-oxygen network structure, the increase of glass density and the decrease of molar volume. Thus, the effects of $B\emptyset_4^-$ and NBO on properties are synergistic rather than independent.

O-O interactions

The pair distribution function of the O-O interactions in the structure of potassium borate glass is shown in the Fig. 5, left. As can be seen from the figure, with the increase of K_2O content, the distance of the first coordination shell of O-O interactions increases from 2.40 to 2.42 Å, indicating that the addition of K_2O elongates the O-O distance. The research of Umesaki et al. [22] also supports this conclusion. But the reason for the increasing O-O distance is still unclear. In this work, atomic labeling method is used to yields three types of O-O interactions: BO-BO, BO-NBO, and NBO-NBO, as shown in Fig. 5, right. In $0.40K_2O{\cdot}0.60^{11}B_2O_3$ glass, the BO-BO interaction has the highest content, accounting for about 55.02%, followed by BO-NBO and NBO-NBO, accounting for 28.84% and 16.14%, respectively. It is worth noting that the distances of the three types of O-O interactions are basically the same, all located at 2.42 Å. This indicates that there is little correlation between the content of NBO and the O-O distance. In $K_2B_4O_7$ crystals containing $B\emptyset_4^-$ and BO_3, the O-O distance in $B\emptyset_4^-$ is about 2.43 Å, and the O-O distance in BO_3 is about 2.37 Å, indicating that the increase in the O-O distance in the glass is related to $B\emptyset_4^-$. In summary, with the increase of K_2O content in potassium borate glass, the $B\emptyset_4^-$ content gradually increases, although the O-B-O bond angle decreases (Fig. S5), and the ^{4}B-O distance still increases, so the O-O distance increases. Therefore, the density increase of potassium borate glass is mainly related to the content of NBO and $B\emptyset_4^-$, and has no direct correlation with the O-O effect.

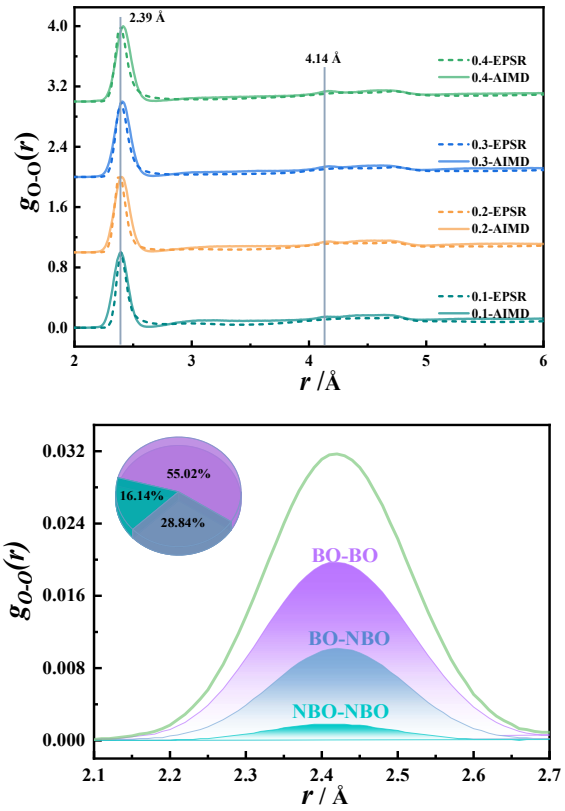

Fig. 5. left: Pair distribution function of O-O interaction in xK$_2$O·(1-x)^{11}B$_2$O$_3$ (0.1≤ x ≤ 0.4) glass obtained by EPSR and AIMD methods, right: pdf diagram of BO-BO, BO-NBO and NBO-NBO interactions in the first coordination layer of O-O interaction in 0.40K$_2$O·0.60^{11}B$_2$O$_3$ glass

K-O Interaction

The first coordination layer distance of K-O interaction in xK$_2$O·(1-x)^{11}B$_2$O$_3$ (0.1≤ x ≤ 0.4) glass is 2.835, 2.815, 2.735 and 2.715 Å, respectively, and the K-O distance decreases gradually with the increase of K$_2$O content. The interaction between K-BO and K-NBO was obtained by atomic labeling method. Fig. 6(a) is the pdf diagram of the first coordination layer of K-O interaction. It can be seen from the diagram that the relative content of K-BO and K-NBO interaction is very close, at 50.99% and 49.01% respectively, with bond lengths of 2.80 and 2.71 Å. This suggests that K$^+$ and NBO form a stronger bond. However, the distance between K-BO and K-NBO in similar component potassium borate crystals is close, as shown in Fig. 6(b). Fig. 6(c) shows the variation of the content of K-BO and K-NBO interactions in xK$_2$O·(1-x)^{11}B$_2$O$_3$ (0.1≤ x ≤ 0.4) glass. As the content of K$_2$O increases, the content of K-BO gradually decreases, while the content of K-NBO gradually increases. The turning point is x = 0.20. This point also happens to be the maximum point of the K-O coordination number, as shown in Fig. S2. When x = 0.40, the content of K-BO and K-NBO interactions are

very close. The structure image in Fig. 6 shows snapshots of $0.10K_2O{\cdot}0.90^{11}B_2O_3$ and $0.40K_2O{\cdot}0.60^{11}B_2O_3$ glass when K^+ is 8 coordinated. In the $0.10K_2O{\cdot}0.9011B_2O_3$ glass, K^+ mainly coordinates with BO. As the K-NBO interaction increases, in the $0.40K_2O{\cdot}0.60^{11}B_2O_3$ glass, K^+ coordinates with four NBOs and four BOs. Therefore, as the content of K_2O increases, the content of NBO increased, and the structural units containing NBO increased, so the interaction of K^+ with NBO increases. In lithium borate glass, the content of NBO also increases with the increase of Li_2O content [55], the results show that both Li_2O and K_2O will destroy the ring structure of B_2O_3 glass and gradually transform it into a "molecular" structural unit containing NBO. Kamitsos et al. [56] study on the far infrared spectral region of $K_2O{\cdot}2B_2O_3$ glass shows that potassium ion exists two vibration modes: L bands (Low frequency) and H bands (High frequency). Combined with the research of Bray et al. [57], the H bands may be corresponding to the vibration associated with K-NBO, the L bands corresponding to the vibration associated with K-BO. When x = 0.33, in our work, the relative content of K-NBO is about 0.41, and the results from Kamitsos et al., [56] is about 0.57±0.05. This difference is mainly caused by the error of different research methods.

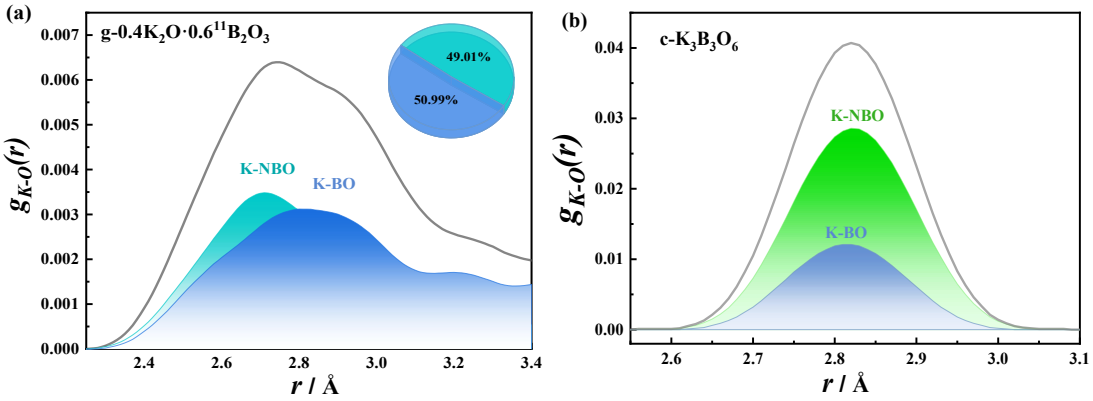

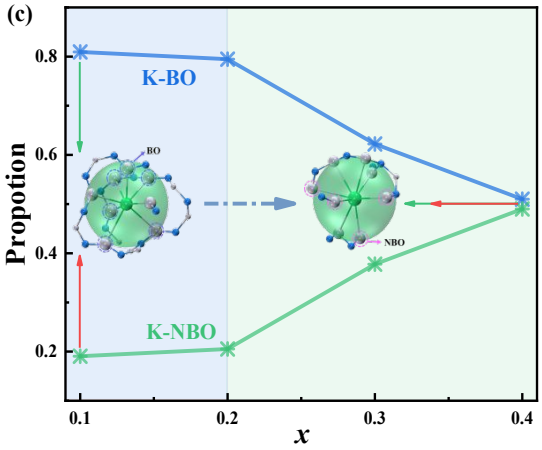

Fig. 6. (a) The distribution of K-BO and K-NBO interactions in the first coordination layer of the K-O interaction in $0.40K_2O{\cdot}0.60^{11}B_2O_3$ glass, the fan chart on the right shows the percentage of each atom-pair interaction; (b) The distribution of K-BO and K-NBO interactions in the first coordination layer of the K-O interaction in $K_3B_3O_6$ crystal ; (c) Changes in the relative contents of K-BO and K-NBO interactions in $x^{11}K_2O{\cdot}(1\text{-}x)B_2O_3$ ($0.1 \leq x \leq 0.4$) glass.

3.2.3. Rings and cavities structure analysis

The ring distribution of $x^{11}K_2O{\cdot}(1\text{-}x)B_2O_3$ (x = 0.10, 0.20, 0.30, 0.40) glass is shown in Fig. 7. As seen from the figure, the potassium borate glass contains numerous four-membered rings, six-membered rings, eight-membered rings, ten-membered rings, and twelve-membered ring structures. When $0.10 \leq x \leq 0.30$, initially, a structural transformation mainly occurs from a boroxol ring to a six-membered ring containing a $B\emptyset_4^-$, as shown in Fig. S7. With the increase of K_2O content, the six-membered ring containing one $B\emptyset_4^-$ is further transformed into a six-membered ring containing two $B\emptyset_4^-$ tetrahedrons (Fig. S7), and the conversion process from the boroxol ring to the diborate unit and the eight-membered ring occurs, as shown in Fig. 8. Finally, most ring structures are connected by sharing the B-O bond, resulting in large ring reunion, as shown in Fig. S6, three six-membered rings. When $0.30 < x \leq 0.40$, the large ring structures decrease significantly, the six-membered rings increase obviously. Moreover, metaborate chains and rings, pyroborate units began to appear, which including more NBO. The agglomeration phenomenon of ring structure disappeared, and the ring structure was evenly dispersed in the whole system. Raman experiment results also show that when x = 0.40, the metaborate chains increase obviously and the ring structure depolymerizes [20]. Fig. 7 shows the ring size distribution of $x^{11}K_2O{\cdot}(1\text{-}x)B_2O_3$

(x = 0.10, 0.20, 0.30, 0.40) glass. As seen from the figure, the system with the lowest number of rings is $0.1K_2O{\cdot}0.9^{11}B_2O_3$ glass. The system with the largest number of rings is $0.3K_2O{\cdot}0.7^{11}B_2O_3$ glass, wherein the six-membered rings are the most numerous, accounting for about 51%. The system with the most six-membered rings is $0.4K_2O{\cdot}0.6^{11}B_2O_3$ glass, accounting for 75% of the total number of rings. Therefore, the increase in the K_2O content causes the ring structure in the potassium borate glass to first increase and then decrease, with the turning point being x = 0.3; When x = 0.3, the tetracoordinated boron content is the highest, resulting in the strongest network connectivity and the largest number of rings [19, 20]. When x > 0.3, the ring structure depolymerizes, the content of large rings decreases, the content of six-membered rings increases, and the ring structure becomes evenly dispersed.

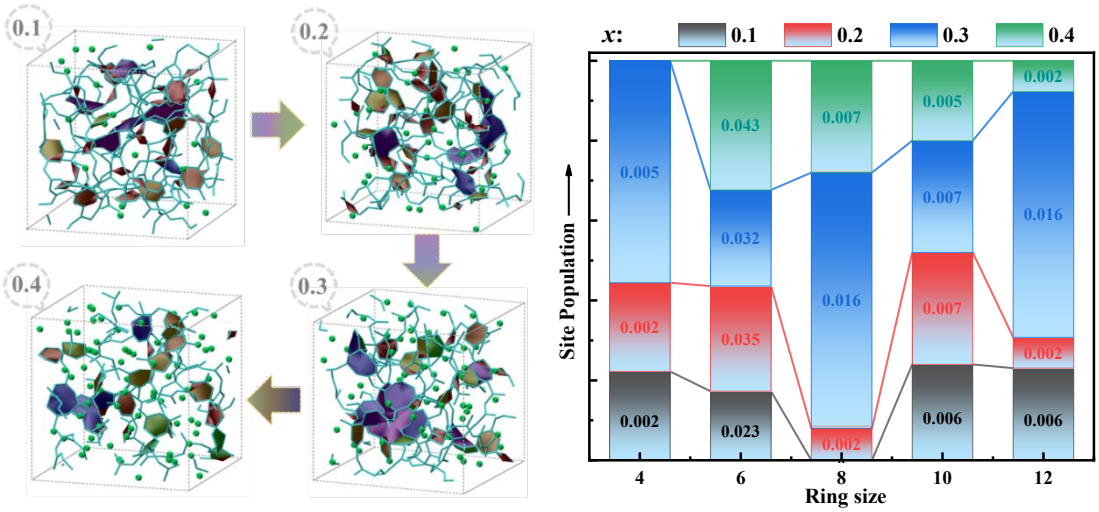

Fig.7. Rings and ring size distribution in simulated box of of $x{K_2O}{\cdot}(1\text{-}x)^{11}B_2O_3$ ($0.1 \leq x \leq 0.4$) obtained by AIMD methods

(a)

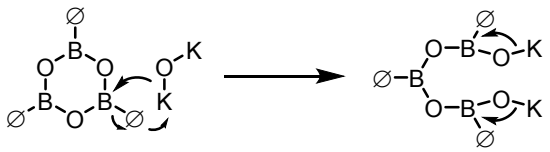

(b)

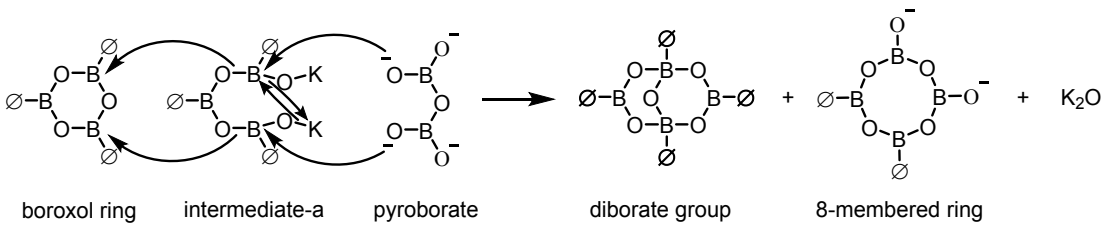

Fig. 8. Schematic diagram of the conversion mechanism between boroxol ring and diborate group, 8-membered ring

The cavities distribution of xK$_2$O·(1-x)^{11}B$_2$O$_3$ glass obtained by the domain-based method [48] is shown in Fig. 9, with all components having a cutoff radius of 2.0 Å. With the increase of K$_2$O content, the cavities occupancy of xK$_2$O·(1-x)^{11}B$_2$O$_3$ (x = 0.10, 0.20, 0.30, 0.40) glass are 7.3%, 6.9%, 5.6%, and 5.2% respectively, the cavity volumes were 399, 379, 277 and 234 Å^3, respectively. The cavities show a decreasing trend. This phenomenon of decreasing cavities occupancy with the increase of metal ion content also exists in sodium thioarsenate and silver thioarsenate glass [58-60].

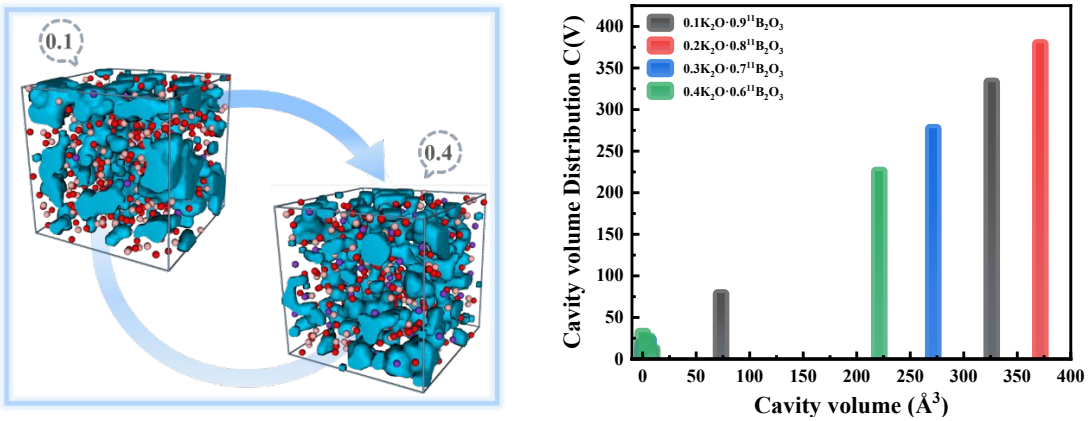

Fig. 9. The cavities distribution and cavities volume distribution histogram of xK$_2$O·(1-x)^{11}B$_2$O$_3$ ($0.1 \leq x \leq 0.4$) glass

3.3 Transport of K$^+$ in Glassy Materials

The study of the ion transport pathway of K$^+$ in borate glassy materials and the structural factors that influence the ion transport rate are essential for improving the performance of potassium solid-state batteries and developing new K$^+$ batteries. Fig. S8 shows an animation of the K$^+$ transport process in 0.40K$_2$O·0.60^{11}B$_2$O$_3$ glassy material. An interesting phenomenon observed is that the transport pathway and sites for adjacent K$^+$ ions are almost identical. However, the transmission rate of K$^+$ during the transmission process is affected by the boron-oxygen network structure. The structural reasons that affect the transport path and rate of potassium ions were analyzed in the following content.

Fig. 10, (a) shows the time trajectory of four K^+ ions at the 150th frame. The denser the trajectory points, the slower the ion transport. According to Fig. S8, the transport of 1# and 3# K^+ is slow, and the transport of 2# and 4# K^+ is faster. This study suggests that the structural factors influencing the K^+ transport rate may include the following points: (1) Coordination number and type of K^+. Fig. 10, (b) shows the coordination distribution of four types of K^+ at frame 150. The NBO/CN ratio (the number of NBOs coordinated with K^+ divided by the total coordination number of that K^+) of 1 to 4# K^+ is 0, 1, 0.4, and 0.4, respectively. Therefore, one of the structural reasons for the faster transport rate of 2# compared to 1# K^+ is that all oxygen atoms coordinated with 2# K^+ are NBOs. It is worth noting that ions 3# and 4# K^+ have the same NBO/CN ratio, but the transport rate of ion 4# is significantly higher than that of 3# K^+. Therefore, besides coordination number and coordination type, there are other factors that influence ion transport. (2) Structural units. Fig. 10, (c) shows the distribution of surrounding structural units for K^+ ions at the 150th frame. It can be observed that 3# K^+ is mainly surrounded by ring-type structures, such as six-membered rings containing $BØ_4^-$ tetrahedra and complex eight-numbered rings. On the other hand, 4# K^+ is mainly surrounded by simple chain-type structures, such as orthoborate units and metaborate units. Therefore, the presence of chain-type structures enhances the facilitation of K^+ transport. (3) Distribution of cavities. As shown in Fig. 10, (d), 1# and 3# K^+ ions are at some distance from the adjacent cavity, so they transport slowly at first. In contrast, 2# and 4# K^+ are directly attached to the cavity, so they are initially transported faster. Akola et al. [59, 60] also suggests that the cavity adjacent to Ag^+ serve as diffusion sites. The data at the 600th frame in Fig. S9 precisely verifies the above analysis results.

In conclusion, the structural factors that influence K^+ transport in potassium borate glass are not singular but rather the result of multiple factors working together. Firstly, the content of NBOs plays a significant role, with a higher NBO content leading to faster K^+ transport. Secondly, the presence of chain-type structural units, such as metaborate-rings and orthoborate chains, which predominantly contain NBOs, facilitates K^+ transport. It should be noted that these chain-type structural units are considered as "molecular-type" structures, as shown in Fig. S6. The structural statistical results reveal

the absence of "molecular-type" structures for x = 0.1 and 0.2, with only a limited presence of $B\emptyset_2O^-$ chain structures observed for x = 0.3, while a significant abundance of metaborate units and orthoborate chains exist for x = 0.4. The distribution of cavity regions also plays a crucial role in ion transport dynamics. The availability of cavity structures surrounding K^+ is essential for diffusion, and a more homogeneous distribution of these regions facilitates efficient K^+ transport. Based on our analysis findings, this study employed AIMD simulations to calculate the diffusion coefficients of K^+ in $x{K_2}O\cdot(1\text{-}x)^{11}B_2O_3$ (x = 0.10, 0.20, 0.30, 0.40) glasses as presented in Table 2, The relevant fitting curves are shown in Fig. S10. It is evident from the results that the diffusion coefficient of K^+ ions gradually increase with an elevated content of K_2O in the glass. This conclusion further substantiates our previous analysis. In other words, the increase of K_2O content in potassium borate glass leads to the increase of NBO content (Fig. S4) and the increase of chain structure, and the cavities distribution became more and more uniform (Fig. 9). These structural changes all contributed to the transport of potassium ions and increased the diffusion coefficient of potassium ions under the action of electric field. The positive correlation about the contents of NBO, chain structure units in potassium borate glass on the transport rate of K^+ ions was established. The study of Kamitsos et al. [61] showed that the diffusion of Li^+ in lithium borate glass is mainly through the NBO site, and in the range of $0.2 \leq x$ (mol $Li_2O\%$) $\leq$ 0.4, with the increase of lithium oxide content, the content of NBO also increases, and the diffusion coefficient of lithium ion also shows an increasing trend, which is the same as that of potassium ion diffusion in potassium borate glass.

Table 2

Diffusion coefficient, error and fitting equations of K^+ in $x{K_2}O\cdot(1\text{-}x)^{11}B_2O_3$ ($0.1 \leq x \leq 0.4$) glass

Sample	D ($cm^2/s\times10^{-5}$)	Error($cm^2/s\times10^{-5}$)	Equations
$0.10{K_2}O\cdot0.90^{11}B_2O_3$	3.13	0.040	$MSD = 0.0013 * t - 0.48$
$0.20{K_2}O\cdot0.80^{11}B_2O_3$	6.43	0.086	$MSD = 0.0026 * t + 0.34$
$0.30{K_2}O\cdot0.70^{11}B_2O_3$	13.25	0.075	$MSD = 0.0053 * t - 1.48$
$0.40{K_2}O\cdot0.60^{11}B_2O_3$	17.90	0.055	$MSD = 0.0072 * t - 2.00$

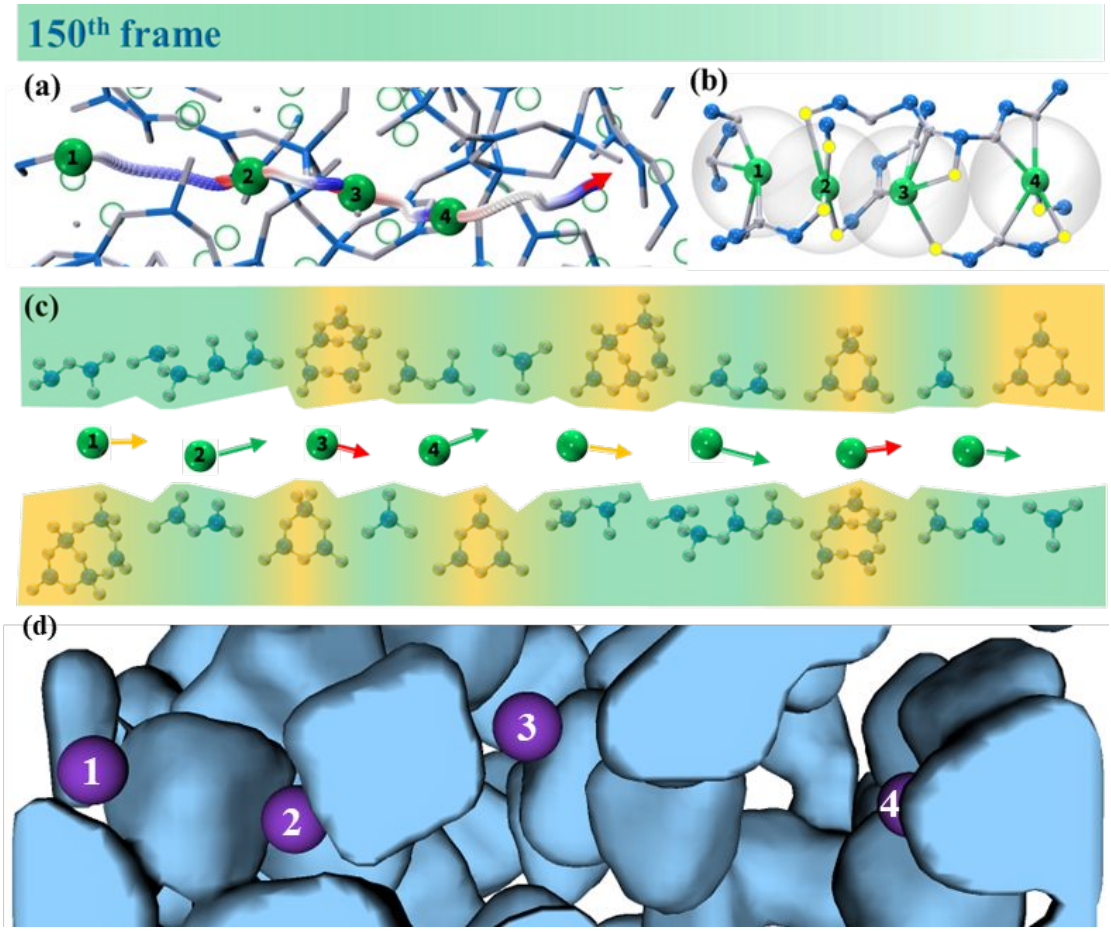

Fig. 10. Transport path of K^+ ions in $0.40K_2O{\cdot}0.60^{11}B_2O_3$ glass: (a) Time trajectory diagram of K^+ at frame 150; (b) K-O coordination map at frame 150, with bright yellow spheres representing NBO; (c) The distribution of structural units around K^+ at frame 150; (d) Map of the cavity's distribution around the four potassium atoms

4. Conclusions

In potassium borate glass, with the increase of K_2O content, $B\emptyset_3$ content decreases, $B\emptyset_4^-$ content increases first and then decreases, and $B\emptyset_{(3-a)}O_a^{-a}$ $_{(a=1\text{ or }2)}$ content increases. With the increase of $B\emptyset_4^-$, the three-dimensional connectivity of the network structure of the glass is enhanced. With the increase of $B\emptyset_{(3-a)}O_a^{-a}$ $_{(a=1\text{ or }2)}$, the content of NBO also increases, and the structure of the boron-oxygen network becomes dispersed. The maximum point of $B\emptyset_4^-$ content (x = 0.3) is also the point with the highest number of rings, density and atomic density. Potassium borate glass contains more B-O bond types than similar component crystals, and the bond lengths of ^{3}B-BO, ^{4}B-BO and ^{3}B-NBO are longer than those of corresponding crystals, so the boro-oxygen network structure

is looser than that of similar component crystals. Additionally, both the crystal and the glass exhibited a reduction in B-O bond length with an increase in NBO, while an increase in ^{4}B resulted in elongation of the B-O bond.

The structural factors affecting K^+ transport rate in $x K_2O \cdot (1-x)^{11}B_2O_3$（$x$ = 0.10, 0.20, 0.30, 0.40） glass mainly include: (1) NBO content, the higher the value, the faster the K^+ transport. (2) Chain structure unit, the more the structural unit, the faster the K^+ transport. (3) Cavity distribution, the more uniform the cavity distribution, the more conducive to K^+ transport. With the increase of K_2O content, the diffusion coefficient of K^+ in glass increases gradually. This study provides reference information for understanding the structure of potassium borate glass and for designing and preparing potassium ion glass solid electrolyte.

Author contributions

Lulu Song performed sample preparation, characterization, Ab initio molecular dynamics simulation, data analysis and manuscript writing. Alex C. Hannon A performed neutron diffraction experiments and manuscript revision. Steve Feller participated in manuscript revision. Ruirui Liu participated in Ab initio molecular dynamics simulation, Peyton McGuire participated in sample preparation, Bo Zhang participated in data analysis, Yongquan Zhou participated in manuscript revision, Wu Li supervised and revised manuscript, Fayan Zhu designed the study, supervised and revised manuscript.

Conflicts of interest

There are no conflicts to declare

Acknowledgements

We thank the Qinghai Province "High-end Innovative Talents Plan" (E240HX1001), 2022 Qinghai Province "Kunlun Talent·High-end Innovation and Entrepreneurship talent" program - Training team (E33EHX04), Qinghai Province

innovation platform construction project (no. 2024-ZJ-T01) and the US National Science Foundation (DMR-RUI 2203142) project for financial support and the Science and Technology Facilities Research Council (STFC) for beam-time on SANDALS (No. 2010510).

References

1 E.O. Taha, A. Saeed, *Sci. Rep*. 2023, 13, 12260.
2 A.E. Harby, A.E. Hannora, A.M. Ali, et al., *Sci. Rep*. 2023, 13, 12498.
3 A.R. Ghazy, B.M. Elmowafy, A.M. Abdelghany, et al., *Sci. Rep*. 2023, 13, 7292.
4 M. Fayaz, S. Ali, S. Bibi, et al., *Ceram. Int*. 2023, 49, 24690-24695.
5 J. Banerjee, G. Ongie, J. Harder, et al., *J Non Cryst Solids*. 20063, 52, 674-678.
6 J.F. Wang, P. Liang, *J. Chem. Thermodyn*. 2019, 134, 1-4.
7 A.M.A. Ghany, A.S.A. Khadra, M.S. Sadeq, *J Non Cryst Solids*. 2020, 548, 120320.
8 M.I. Sayyed, M.A. Abdo, H.E. Ali, et al., *Ceram. Int.* 2022, 48, 24310-24318.
9 S.A.M. Issa, M. Ahmad, H.O. Tekin, et al., *Results Phys*. 2019, 13, 102165.
10 M.I. Sayyed, M.A. Abdo, H.E. Ali, et al., *Ceram. Int.* 2022, 48, 30817-30825.
11 H. Aboud, H. Wagiran, R. Hussin, et al., *Appl Radiat Isot.* 2014, 90, 35-39.
12 B. Pandit, E.S. Goda, M. Ubaidullah, et al., *Ceram. Int.* 2022, 48, 28856-28863.
13 R. Balaji Rao, R.A. Gerhardt, N. Veeraiah, *J Phys Chem Solids.* 2008, 69, 2813-2826.
14 A.E. Omar, A.M. Ibrahim, T.H. Abd El-Aziz, et al., *J Biomed Mater Res B.* 2021, 109, 1059-1073.
15 R.E. Youngman, J.W. Zwanziger, *J. Phys. Chem*. 1996, 100, 16720-16728.
16 W.L. Konijnendijk, J.M. Stevels, *J. Non Cryst. Solids.* 1975, 18, 307–331.
17 E. Kamitsos, M.A. Karakassides, G.D. Chryssikos, Phys. Chem. Glasses. 1989, 30, 229–234.
18 G.D. Chryssikos, E. Kamitsos, M.A. Karakassides, *Phys. Chem. Glasses*. 1990, 31, 109–116.
19 A.A. Osipov, L.M. Osipova, R.T. Zainullina, *Phys. Chem. Glasses: Eur. J. Glass Sci. Technol. B.* 2015, 56, 248-254.
20 O.N. Koroleva, M.V. Shtenberg, *J Non Cryst Solids*. 2023, 601, 122053.
21 A.C. Wright, R.N. Sinclair, C.E. Stone, et al., *Phys. Chem. Glasses: Eur. J. Glass Sci. Technol. B.* 2012, 53, 191-204.
22 K. Handa, Y. Kitab, S. Kohara, et al., *J. Phys. Chem. Solids.* 1999, 60, 1465–1471.
23 B. Stevensson, Y. Yu, M. Edén, *Phys. Chem. Chem. Phys*. 2018, 20, 8192-8209.
24 G. D. Chryssikos, E. I. Kamitsos, A. P. Patsis, et al.,*Mater. Sci. Eng*. 1990, B7, 1–4.
25 E. I. Kamitsos, G. D. Chryssikos, *J. Mol. Struct.* 1991, 247, 1–16.
26 T. Liu, B. Duan, Y.Q. Li, et al., *J Non Cryst Solids.* 2023, 604, 122134.
27 V. Dua, S.K. Arya, K. Singh, *J. Mater. Sci.* 2023, 58, 8678-8699.
28 S.C. Colak, G. Kilic, *J. Mater. Sci. Mater. Electron.* 2022, 33, 21852-21863.

29 N. Effendy, H.A.A. Sidek, M.K. Halimah, *Chinese J. Phys*. 2022, 75, 1-13.
30 L.L. Song, Y.X. Wang, A.C. Hannon, et al., *J Non Cryst Solids.* 2023, 616, 122478.
31 H. Bradtmüller, A. Gaddam, H. Eckert, et al., *Acta Mater.* 2022, 240, 118318.
32 E.D. Zanotto, J.E. Tsuchida, J.F. Schneider, et al., *Int. Mater. Rev*. 2015, 60, 376-391.
33 S. Lan, L. Zhu, Z. Wu, et al., *Nat. Mater*. 2021, 20, 1347-1352.
34 J. Ge, Y. Gu, Z. Yao, et al., *J Mater Sci Technol*. 2024, 176, 224-235.
35 A.C. Hannon, *Nucl. Instrum. Methods Phys. Res.,Sect. A*. 2005, 551, 88-107.
36 A. Hannon, W. Howells, A. Soper, *Inst. Phys. Conf. Ser.* 1990, pp. 193-211.
37 E. Lorch, *Phys. Solid State.* 1969, 2, 229.
38 A.C. Hannon, *J Non Cryst Solids.* 2016, 451, 56-67.
39 A.C. Hannon, A.S. Gibbs, H. Takagi, *J Appl Crystallogr*. 2018, 51, 854-866.
40 J. Hutter, M. Iannuzzi, F. Schiffmann, et al., *Rev. Comput. Mol. Sci.* 2014, 4, 15-25.
41 Z. Wu, R.E. Cohen, *Phys. Rev. B.* 2006, 73, 235116.
42 L. Martínez, R. Andrade, E.G. Birgin, et al., *J Comput Chem*. 2009, 30, 2157-2164.
43 D.V. Oliveira, J. Laun, M.F. Peintinger, et al., *J Comput Chem*. 2019, 40, 2364-2376.
44 S. Goedecker, M. Teter, J. Hutter, *Phys. Rev. B.* 1996, 54, 1703.
45 S. Nosé, *Mol Phys.* 1984, 52, 255-268.
46 W.G. Hoover, *Phys Rev A.* 1985, 31, 1695.
47 S. Le Roux, P. Jund, *Comput. Mater. Sci.* 2010, 49, 70-83.
48 I. Heimbach, F. Rhiem, F. Beule, et al., *J Comput Chem.* 2017, 38, 389–394.
49 W. Humphrey, A. Dalke, K. Schulten, *J. Mol. Graph. Model*. 1996, 14, 33-38.
50 A.K. Soper, *Phys. Rev. B.* 2005, 72, 104204.
51 A. Hannon, D. Grimley, R. Hulme, et al., *J Non Cryst Solids.* 1994,177, 299-316.
52 P.A. Johnson, A.C. Wright, *J Non Cryst Solids.* 1982, 50, 281 - 311.
53 R.L. Mozzi, B.E. Warren, *J Appl Crystallogr.* 1970, 3, 251-257.
54 N.P. Lower, J.L. McRae, H.A. Feller, et al., *J Non Cryst Solids.* 2001, 293, 669-675.
55 G. Lelong, L. Cormier, L. Hennet, et al., *Inorg. Chem.* 2021, 60, 798-806.
56 E.I. Kamitsos, A.P. Patsis, G.D. Chryssikos. *J Non Cryst Solids*. 1993, 152, 246-257.
57 J. H. Zhong, P. J. Bray. *J Non Cryst Solids*. 1989, 111: 67-76.
58 M. Kassem, T. Bounazef, D. Fontanari, et al., *Inorg. Chem.* 2020, 59, 16410-16420.
59 J. Akola, P. Jóvári, I. Kaban, et al., *Phys. Rev. B.* 2014, 89, 064202.
60 J. Akola, B. Beuneu, R.O. Jones, et al., *J. Phys. Condens. Matter.* 2015, 27, 485304.
61 C.P. Varsamis, A. Vegiri, E.I. Kamitsos, *Phys. Rev. B*. 2002, 65, 1-14.